Published in final edited form as:
Vision Res. 2011 January 28; 51(2): 269–279. doi:10.1016/j.visres.2010.08.039.

Morphologies of mouse retinal ganglion cells expressing transcription factors Brn3a, Brn3b, and Brn3c: analysis of wild type and mutant cells using genetically-directed sparse labeling

Tudor Constantin Badea[1,3] and **Jeremy Nathans**[1,2]

[1]Department of Molecular Biology and Genetics, Howard Hughes Medical Institute, Johns Hopkins University School of Medicine, Baltimore, Maryland 21205

[2]Department of Neuroscience, Department of Ophthalmology, Johns Hopkins University School of Medicine, Baltimore, Maryland 21205

[3]Retinal Circuit Development & Genetics Unit, Neurobiology-Neurodegeneration and Repair Laboratory, National Eye Institute, Bethesda, Maryland 20892

Abstract

The mammalian retina contains more than 50 distinct neuronal types, which are broadly classified into several major classes: photoreceptor, bipolar, horizontal, amacrine, and ganglion cells. Although some of the developmental mechanisms involved in the differentiation of retinal ganglion cells (RGCs) are beginning to be understood, there is little information regarding the genetic and molecular determinants of the distinct morphologies of the 15 – 20 mammalian RGC cell types. Previous work has shown that the transcription factor Brn3b/Pou4f2 plays a major role in the development and survival of many RGCs. The roles of the closely related family members, Brn3a/Pou4f1 and Brn3c/Pou4f3 in RGC development are less clear. Using a genetically-directed method for sparse cell labeling and sparse conditional gene ablation in mice, we describe here the sets of RGC types in which each of the three Brn3/Pou4f transcription factors are expressed and the consequences of ablating these factors on the development of RGC morphologies.

Keywords

Mouse; Retina Development; Retinal Ganglion Cell; Brn3 Transcription Factors; Dendritic Arbor

1. Introduction

Visual information undergoes a first level of processing in the retina, and the features extracted from the stimulus are conveyed to the brain through parallel channels subserved by 15–20 distinct retinal ganglion cell (RGC) types (Masland, 2001; Ramon y Cajal, 1972; Wassle, 2004 and references within). RGC types can be distinguished by their physiological properties (Barlow et al., 1964; Levick, 1967; Cleland and Levick, 1974a, 1974b; Roska and Werblin, 2001; Troy and Shou, 2002), target nuclei in the brain (Pu & Amthor, 1990a,

Address for editorial correspondence: Dr. Tudor C. Badea, 805 PCTB, 725 North Wolfe Street, Johns Hopkins University School of Medicine, Baltimore, MD 21205, tel: 410-955-4680, FAX: 410-614-0827, tbadea@mail.jhmi.edu, badeatc@mail.nih.gov.

1990b; Rodieck and Watanabe, 1993; Simpson, 1984), patterns of dendritic arborization in the retina (Ramon y Cajal, 1972; Boycott and Wassle, 1974; Levick, 1975; Amthor et al., 1984; Rockhill et al., 2002) and, in a few cases, molecular markers (Siegert et al., 2009; Kim et al., 2010).

RGC typography depends on the classification criteria applied and species studied (Masland and Martin, 2007). Combining information about central brain projections, physiological light responses, and dendritic morphology is highly advanced in cat and primate retinas and has created a detailed picture of RGC types (Rodieck and Watanabe, 1993; Dacey et al., 2003). In the mouse, classification schemes based solely on morphological (Sun et al., 2002; Badea and Nathans, 2004; Kong et al., 2005; Coombs et al., 2006; Volgyi et al., 2009), or physiological (Carcieri et al., 2003; Pang et al., 2003; Zeck and Masland, 2007) criteria have recently been complemented by the discovery of molecular markers for individual RGC cell types (Hattar et al., 2002; Huberman et al., 2008; Kim et al., 2008; Yonehara et al., 2008; Huberman et al., 2009; Siegert et al., 2009; Kim et al., 2010). RGC type-specific expression of fluorescent, immunohistochemical, or enzymatic reporters has further advanced the integration of dendritic morphology, physiology, and projection patterns (Berson et al., 2002; Hattar et al., 2002; Huberman et al., 2008; Kim et al., 2008; Yonehara et al., 2008; Do et al., 2009; Huberman et al., 2009; Yonehara et al., 2009). Finally, genetic manipulations targeted to specific RGC types permit type-specific cell deletion or modification and an analysis of the resulting effect on visual reflexes and behaviors (Guler et al., 2008; Badea et al., 2009a). These results underscore the utility of understanding the molecular genetics and development of RGC types in the mouse retina.

Studying the morphology of RGC dendritic arbors is of interest not only as an aid in cell type classification, but because dendritic morphology relates directly to RGC response properties. In particular, the area of the arbor is closely correlated with the size of the RGC receptive field and the level of dendritic lamination in the inner plexiform layer determines the type of amacrine and bipolar cells from which the RGC receives its input (Boycott and Wassle, 1974; Famiglietti and Kolb, 1976; Amthor et al., 1984; Kim et al., 2008). At present, the molecular mechanisms that specify the area, shape, and stratification level(s) of RGC dendritic arbors are still poorly understood (Yamagata et al., 2002; Fuerst et al., 2008; Yamagata and Sanes, 2008; Badea et al., 2009a; Fuerst et al., 2009).

One family of transcription factors that is expressed in the retina exclusively in RGCs is the Pou4f/Brn3 family of transcription factors (Xiang et al., 1995; Erkman et al., 1996; Gan et al., 1996; Xiang et al., 1996; Xiang et al., 1997; Badea et al., 2009a). The three members of the Brn3 family - Brn3a, Brn3b and Brn3c - are present in partially overlapping subpopulations of RGCs. They are also expressed in primary sensory neurons in the dorsal root and trigeminal ganglia, and in auditory and vestibular hair cells (Brn3c) or their synaptic partners in the vestibular system (Brn3a and Brn3b) (Xiang et al., 1995; Erkman et al., 1996; Gan et al., 1996; Xiang et al., 1996; Xiang et al., 1997). In the retina, targeted deletion of Brn3b results in the loss of 70 – 80% of RGCs, with many of the surviving RGCs exhibiting severe axonal defects (Erkman et al., 1996; Gan et al., 1996; Erkman et al., 2000; Badea et al., 2009a). Deletion of Brn3a specifically in the retina results in a characteristic change in the distribution of RGC dendritic morphologies (Badea et al., 2009a). Deletion of Brn3c does not have a major effect on RGC survival, but the Brn3b and Brn3c double mutant shows an increase in the severity of RGC loss compared to the Brn3b mutant (Wang et al., 2002). Thus, each Brn3 gene plays a distinctive role in RGC development.

Several questions remain open regarding the role of the Brn3 transcription factors in RGC development and type specification. Which RGC types express each of the Brn3 transcription factors? Does Brn3c have a role in RGC development independent of its effects

on cell survival in combination with Brn3b? What are the molecular mechanisms by which the Brn3 proteins regulate RGC cell type specification?

To begin to address these questions, we have developed a strategy in which Cre-mediated recombination of a conditional *Brn3* allele simultaneously excises the Brn3 coding region and activates a previously silent histochemical reporter (alkaline phosphatase; AP) by bringing the AP coding region under the control of the *Brn3* promoter (Badea et al., 2009a and references within). Using this technique under conditions that produce a sparse collection of recombined cells, one can observe and quantify the morphologies of individual RGCs expressing the targeted *Brn3* gene. In addition, by comparing mouse lines in which the conditional *Brn3* allele is paired either with a wild type (WT) allele or with a conventional null allele, one can compare the morphologies of individual RGcs that are either homozygous mutant or heterozygous, respectively, for the *Brn3* gene being manipulated.

In the present study we define the morphological subtypes of RGCs that express *Brn3a*, *Brn3b*, and *Brn3c*, and for each of the *Brn3* genes we quantify a series of parameters that characterize the dendritic morphology in wild type compared to mutant RGCs.

2. Materials and Methods

2.1 Mouse strains and crosses

Mouse lines carrying alleles $Brn3a^{-}$, $Brn3b^{-}$, $Brn3c^{-}$, $Brn3a^{CKOAP}$, $Brn3b^{CKOAP}$, and $R26^{rtTACreER}$ were previously described (Gan et al., 1996; Xiang et al., 1996; Xiang et al., 1997; Badea et al., 2009a, 2009b). The $Brn3c^{CKOAP}$ allele (T. Badea, J. Williams, P. Smallwood, and J. Nathans, manuscript in preparation) is a conditional knock-in AP reporter allele analogous to the $Brn3a^{CKOAP}$ and $Brn3b^{CKOAP}$ alleles described in Badea et al. (2009a).

To obtain sparse Cre-mediated recombination in RGCs, the following crosses were set up: (1) $R26^{rtTACreER/+rtTACreER/+}$;$Brn3a^{+/-}$ male × $Brn3a^{CKOAP/CKOAP}$ female, (2) $R26^{rtTACreER/+}$;$Brn3b^{+/-}$ male × $Brn3b^{CKOAP/CKOAP}$ female, and (3) $R26^{rtTACreER/+}$;$Brn3c^{+/-}$ male × $Brn3c^{CKOAP/CKOAP}$ female. Conception date was determined by examining the copulation plug, and pregnant females were moved to cages with food pellets containing Doxycyline (1.75 mg/gram) at gestational day 2–4. At gestational day 11 – 13, 100 – 250 μg of 4-hydroxytamoxifen in sunflower seed oil vehicle was delivered by intraperitoneal injection, and the doxycycline diet was continued until birth (Table 1). A detailed description of this protocol can be found in Badea et al. (2009b).

2.2 Histochemistry

At 4–8 weeks after birth, mice of the six desired genotypes ($R26^{rtTACreER/+}$;$Brn3a^{CKOAP/+}$, $R26^{rtTACreER/+}$;$Brn3a^{CKOAP/-}$, $R26^{rtTACreER/+}$;$Brn3b^{CKOAP/+}$, $R26^{rtTACreER/+}$;$Brn3b^{CKOAP/-}$, $R26^{rtTACreER/+}$;$Brn3c^{CKOAP/+}$, and $R26^{rtTACreER/+}$;$Brn3c^{CKOAP/-}$) were anesthetized with ketamine and xylazine, and fixed with 4% paraformaldehyde in PBS by intracardiac perfusion. Retinas were dissected, flat mounted, and histochemically stained for AP as previously described (Badea et al., 2003). Retina flat mounts were dehydrated in an ethanol series and cleared and mounted in benzyl benzoate: benzyl alcohol (2:1).

2.3 Image collection and analysis

Montages of the whole retina were generated at 5X magnification using a Zeiss Z1 Imager microscope equipped with a motorized xyz stage. Individual RGCs were imaged under DIC/

Nomarsky transmitted light, and z-stacks were collected with a 20X objective (3.125 pixels/μm) at 1 μm vertical (z dimension) intervals. For each RGC dendritic arbor, the area and the inner (vitreal) and outer (scleral) limits of the stratification depth within the inner plexiform layer (IPL) were determined (Badea et al., 2003; Badea et al., 2009a, 2009b; Fig. 1H,I). Scatter plots were prepared to assess the relationships among the measured parameters using MatLab and Excel. Individual examples of distinct morphological types were reconstructed (i.e. traced) using Neuromantic freeware (www.rdg.ac.uk/neuromantic/).

3. Results

3.1 Genetically-directed sparse labeling of RGCs

We used a Cre recombinase-estrogen receptor ligand binding domain fusion protein (CreER) to effect recombination of a pair of *loxP* target sites in each *Brn3* conditional allele to visualize the dendritic arbors of RGCs expressing each Brn3 transcription factor (Badea et al., 2003; Badea and Nathans, 2004). For improved control over recombination efficiency at early developmental time points, we used a recently generated $R26^{rtTACreER}$ knock-in allele, in which Cre recombinase activity is under two levels of pharmacologic control: expression of CreER is regulated at the transcriptional level by the doxycycline-dependent activation of the reverse tetracycline trans-activator (rtTA), and nuclear import of CreER is controlled, in a dose-dependent manner, by 4–hydroxytamoxifen (4-HT) (Badea et al., 2009b).

To specifically label RGCs expressing *Brn3a*, *Brn3b*, or *Brn3c*, we used the previously described $Brn3a^{CKOAP}$ and $Brn3b^{CKOAP}$ conditional knock-in AP reporter alleles, and an analogous, newly generated $Brn3c^{CKOAP}$ allele (Badea, Williams, Smallwood, and Nathans, manuscript in preparation). Using an optimized doxycycline and 4-HT delivery protocol (Badea et al., 2009b), we induced sparse recombination at each of the three $Brn3^{CKOAP}$ alleles, resulting in excision of the coresponding Brn3 coding region and its replacement with AP ($Brn3^{AP}$). As noted in the Introduction, the neurons that have undergone Cre-mediated recombination become heterozygous for the targeted transcription factor if the *Brn3* allele on the homologous chromosome is WT (starting genotype $Brn3^{CKOAP/+}$; final genotype $Brn3^{AP/+}$), or they become null for the targeted transcription factor if the Brn3 allele on the homologous chromosome is a conventional null mutation (starting genotype $Brn3^{CKOAP/-}$; final genotype $Brn3^{AP/-}$). In either case, the surrounding cells remain phenotypically WT. Retinas from mice with each of the six relevant genetic backgrounds ($R26^{rtTACreER/+}$;$Brn3a^{CKOAP/+}$, $R26^{rtTACreER/+}$;$Brn3a^{CKOAP/-}$, $R26^{rtTACreER/+}$;$Brn3b^{CKOAP/+}$, $R26^{rtTACreER/+}$;$Brn3b^{CKOAP/-}$, $R26^{rtTACreER/+}$;$Brn3c^{CKOAP/+}$, $R26^{rtTACreER/+}$;$Brn3c^{CKOAP/-}$) were histochemically stained in flat mount preparations for AP activity (Fig. 1A–F). Since all of the data presented in this study used the $R26^{rtTACreER}$ allele as a source of Cre recombinase, we will refer hereafter only to the *Brn3* alleles in describing the genotype of each line, e.g. $Brn3a^{CKOAP/+}$ instead of $R26^{rtTACreER/+}$;$Brn3a^{CKOAP/+}$. Panels A–C in Fig. 1 show examples of retina flat mounts in which the AP+ RGCs are heterozygous for the indicated Brn3 transcription factor, whereas panels D–F in Fig. 1 show AP+ RGCs that lack the indicated transcription factor. Many aberrant AP+ neurites are seen following loss of *Brn3b* (Fig. 1E,F), consistent with our earlier experiments in which recombination was driven by a Pax6-αCre transgene (Badea et al., 2009a). In all of the figures the labels refer to the genotype of the mouse (e.g. $Brn3b^{CKOAP/-}$) rather than the genotype of the individual AP-expressing RGCs (e.g. $Brn3b^{AP/-}$).

3.2 General characteristics of RGCs: morphologic and parametric analyses

A total of 580 RGCs were analyzed. They were obtained from 38 retinas (Table 1) and were distributed approximately equally among the six genotypes. Individual RGC axons and

dendrites were imaged using DIC/Nomarski optics under transmitted light, and successive optical sections where collected at 1 μm vertical (z dimension) intervals. To classify RGCs based on dendrite morphology, cells were first separated into monostratified or bistratified types based on the absence or presence of two well-separated, flat dendritic arbors. Fig. 1G and Table 2 show that the proportion of monostratified and bistratified types varies among WT RGCs that express the different Brn3 genes, with Brn3b-expressing RGCs showing the lowest proportion of bistratified cells and Brn3c-expressing RGCs showing the highest proportion. The effects of deleting each Brn3 gene on the ratio of monostratified to bistratified RGCs are described in section 3.7. For each dendritic arbor, the inner (vitreal) and outer (scleral) limits – abbreviated as ID (inner distance) and OD (outer distance), respectively - were measured (Fig. 1H). ID and OD were normalized to the total thickness of the IPL at the same (x,y) position. Finally, the arbor area was measured by constructing a bounding polygon with vertices defined by the most distal points along the dendritic tree (Fig. 1I).

Fig. 2 shows examples of dendritic arbors imaged at various z-axis focal planes (panels A and B), together with a series of reconstructed $Brn3^{AP/+}$ RGCs (panel C) and $Brn3^{AP/-}$ RGCs (panel D). Each reconstructed RGC in Fig. 2C and D is shown *en face* with respect to the plane of the retina (upper image) and from the side (lower image), and is assigned a lower case letter (a through x). The images in panels A and B correspond, respectively, to reconstructed cell c in panel C and cells w and x in panel D. In panel C, the colored borders and their associated labels indicate which RGC morphologies are characteristic of $Brn3a^{AP/+}$, $Brn3b^{AP/+}$, or $Brn3c^{AP/+}$ RGCs; for example, the morphology exemplified by the RGC designated n in Fig. 2C is characteristic of $Brn3a^{AP/+}$ and $Brn3c^{AP/+}$ RGCs. The genotypes of each RGC in Fig. 2C are indicated in the scatter plots in Figs. 3 and 4, in which area and dendritic stratification parameters are cross-correlated for each RGC in the monostratified and bistratified data sets, respectively. Fig. 2D shows a series of reconstructed $Brn3a^{AP/-}$ and $Brn3b^{AP/-}$ RGCs; their corresponding data points are also indicated in the scatter plots in Figs. 3 and 4. In the text that follows, we will refer to each of these cells by its letter designation; as each cell is discussed, the reader is encouraged to consult both the reconstructed cell image (Fig. 2) and the scatter plots (Figs. 3 and 4).

In general, the quantitative relationships between dendritic arbor area and arbor stratification level show a narrower range of variation within the set of WT bistratified RGCs compared to the WT monostratified RGCs, with the monostratified cells segregating into many distinct clusters across an extended hyper-volume of parametric space (compare Fig. 3A and B vs. Fig. 4A and B). Among monostratified $Brn3b^{AP/+}$ and $Brn3c^{AP/+}$ RGCs, the level of dendritic arborization, as measured by the normalized ID parameter, clusters into two relatively discrete groups when plotted against arbor area (Fig. 3B). Among the monostratified $Brn3b^{AP/+}$ RGCs, these two groups further divide into four subgroups when ID is plotted against OD (Fig. 3A). By contrast, monostratified $Brn3a^{AP/+}$ RGCs show a more continuous distribution across parametric space (Fig. 3A–C).

The thickness of a dendritic arbor in the z-dimension can be determined by subtracting ID from OD (Fig. 3C). This parameter, which can also be inferred from the plots of ID vs OD (Fig. 3A), shows a distinctive distribution for each Brn3 subset (Fig. 3C). For monostratified $Brn3a^{AP/+}$ and $Brn3b^{AP/+}$ RGCs, arbor areas show an inverse correlation with arbor thickness; in other words, arbors with large areas tend to be relatively thin in the z-dimension, whereas arbors with small areas tend to be relatively thick in the z-dimension. Using the (OD-ID)/IPL thickness parameter, monostratified $Brn3b^{AP/+}$ RGC dendritic arbors can be subdivided in three distinct sets, with the thinnest set encompassing all of the arbors with large areas (Fig. 3C).

In sections 3.3 – 3.5 below we present a more detailed description of individual RGC types.

3.3 RGCs with small or asymmetric arbors

A distinct morphologic type of RGC has dendritic arbors that are sector shaped when viewed in the plane of the retina, slope from their origin at the cell body through the full width of the IPL, and end in a flat arbor apposed to the INL (e.g., cell c). This cell morphology, present among both *Brn3a*$^{AP/+}$ and *Brn3b*$^{AP/+}$ RGCs, has been previously described in unbiased morphologic surveys (Sun et al., 2002 - type C6; Badea and Nathans, 2004 - monostratified RGC cluster 6), and has recently been shown to express the molecular marker JamB and to respond selectively to upward motion (Kim et al., 2008; Kim et al., 2010).

A second subset of monostratified RGCs exhibits small, thick, more complex dendritic arbors, and is found only among *Brn3a*$^{AP/+}$ and *Brn3b*$^{AP/+}$ RGCs. RGCs of this general category may belong to several distinct types that are not well resolved with the parameters used here. One morphology belonging to this group exhibits an arbor thickness ((OD-ID)/IPL) of 0.4 – 0.6, is common among *Brn3a*$^{AP/+}$ and *Brn3b*$^{AP/+}$ RGCs, and spans from a normalized ID of ~0.35 to the INL (e.g., cell e). These cells could reasonably be classified as bistratified as their arbors, although not cleanly segregated into two planes, have higher dendritic densities at their inner and outer edges. The remainder of this group consists of RGCs with very dense dendritic arbors. The ones observed among *Brn3b*$^{AP/+}$ RGCs (e.g., cell d) have small areas (mean area = 6,397 μm^2, SD = 2,670 μm^2) and are tightly clustered in parametric space (mean ID/IPL = 0.455; mean thickness = 0.29), suggesting a unique cell type, most likely an “ON” RGC. Similar *Brn3a*$^{AP/+}$ RGCs have large arbor widths ((OD-ID)/IPL = 0.2 – 0.4) and small arbor areas (mean area = 9,436 μm^2, SD = 6,418 μm^2; e.g., cell j), but they span a broader range of stratification levels (ID/IPL = 0.34 – 0.74). Thus, the *Brn3a*$^{AP/+}$ RGCs in this somewhat heterogeneous group very likely comprise both “ON” RGCs as well as “OFF” RGCs (e.g. cell j).

3.4 RGCs with flat, monostratified arbors

The majority of monostratified RGCs have relatively flat arbors. They distribute along the diagonal axis in the ID vs OD plots (Fig. 3A; i.e., ID and OD have similar values), and to the left side of the OD-ID vs area plots (Fig. 3C). All monostratified *Brn3c*$^{AP/+}$ RGCs fall into this category (Fig. 3C).

Based on ID, OD, and area parameters *Brn3c*$^{AP/+}$ RGCs cluster in two distinct groups (Fig. 3A, B). [In the descriptions that follows, we make use of the laminar positions of starburst amacrine cell processes at normalized distances from the inner border of the IPL of ~0.4 and ~0.7; these are indicated in Fig. 3A and B and Fig. 4A by vertical lines; see Haverkamp and Wassle (2000); Morgan et al. (2006); Badea et al. (2009a), for examples of choline acetyltransferase, calretinin and calbindin immunostaining. These landmarks, together with a central band of calretinin immunostaining midway between the starburst amacrine bands, define the junction between the ON and OFF laminae at a normalized distance of ~0.55 from the inner border of the IPL (Euler et al., 1996; Haverkamp and Wassle, 2000; Ghosh et al., 2004; Morgan et al., 2006). Although we have not determined the response properties of the RGCs described here, in the text that follows we take the liberty of provisionally referring to those RGCs with arbors vitreal to the ON/OFF junction at ~0.55 as “ON” RGCs and those RGCs with arbors scleral to that junction as “OFF” RGCs.] The “OFF” *Brn3c*$^{AP/+}$ RGC population has dendritic arbors stratifying between the outer starburst amacrine band and the inner nuclear layer (INL; ID mean=0.83, SD=0.04; OD mean=0.89, SD=0.037), whereas the majority of the dendritic arbors of the “ON” *Brn3c*$^{AP/+}$ RGC population are confined between the inner starburst amacrine band and the ON/OFF boundary (ID mean=0.48,

SD=0.074; OD mean=0.57, SD=0.075). RGCs with similar morphologies to the "OFF" *Brn3c*$^{AP/+}$ RGC population can be seen among both *Brn3a*$^{AP/+}$ and *Brn3b*$^{AP/+}$ RGCs (e.g., cell o), which represents the only cell morphology common to all three Brn3 transcription factors. The "ON" *Brn3c*$^{AP/+}$ RGC morphological type, which is easily recognized in the flat mount view because of its highly ramified and homogeneously distributed dendrite pattern, is also present among *Brn3a*$^{AP/+}$ RGCs (e.g., cell n), but not among *Brn3b*$^{AP/+}$ RGCs.

Flat monostratified *Brn3b*$^{AP/+}$ "OFF" RGCs constitute a more complex set, but they can be subdivided based on arbor stratification levels and areas. The "OFF" *Brn3b*$^{AP/+}$ RGCs stratify between the outer starburst amacrine lamina and the INL with a broad distribution of area values. In addition to morphologies similar to the "OFF" *Brn3c*$^{AP/+}$ RGCs, (e.g., cell o), two larger cells are also seen. Cell f is reminiscent of the melanopsin expressing "OFF" RGC morphology (Hattar et al., 2002; Berson et al., 2010; Ecker et al., 2010), with an extremely large area (87,246 μm^2 for this example) and a sparse dendritic arbor. A second group of large "OFF" RGCs, with dense and straight dendrites is present among both *Brn3a*$^{AP/+}$ and *Brn3b*$^{AP/+}$ RGCs (e.g., cell b), but cannot be separated as a distinct cluster from the smaller o type cells based only on the parameters used here.

"ON" RGCs with flat dendritic arbors most likely represent a mixture of cell types in both the *Brn3a*$^{AP/+}$ and *Brn3b*$^{AP/+}$ RGC sets. Rather than attempting a classification of the different subtypes, we provide below a general description of their morphology, along with some representative examples. The dendritic arbors of "ON" *Brn3b*$^{AP/+}$ RGCs (minimum area = 9,088 μm^2, maximum area = 91,566 μm^2, mean = 38,879 μm^2) are, on average, much larger than their *Brn3a*$^{AP/+}$ (minimum area = 3,823 μm^2, maximum area = 38,877 μm^2, mean = 14,479 μm^2) and *Brn3c*$^{AP/+}$ (minimum area = 4211.4 μm^2, maximum area = 45,075 μm^2, mean = 16,256 μm^2) counterparts. Many "ON" *Brn3b*$^{AP/+}$ RGCs are distinctive in that their dendrites stratify close to the ganglion cell layer (GCL), with ID/IPL generally less than 0.4, whereas the dendrites of "ON" Brn3a$^{AP/+}$ RGCs have a minimal ID/IPL ratio of 0.27, and generally stratify at, or scleral to, the starburst amacrine landmark at 0.4 (Fig. 3A,B). Cells g and i represent examples of flat "ON" *Brn3b*$^{AP/+}$ RGCs with large dendritic arbors stratifying in close proximity to the GCL. These morphologies, like the large "OFF" cell f, are unique to *Brn3b*$^{AP/+}$ RGCs. Based on their areas and stratification levels, cells f and g most likely correspond to the M1 and M2 morphologies, respectively, of intrinsically photosensitive RGCs (Hattar et al., 2002; Berson et al., 2010; Ecker et al., 2010).

One particular type of flat, "ON" dendritic arbor, shared by *Brn3a*$^{AP/+}$ and *Brn3b*$^{AP/+}$ RGCs is exemplified by cell a. The arbor stratifies at the 0.4 IPL starburst amacrine cell landmark, is extremely flat, and, in some examples exhibits isolated recurrent dendrites looping into the "OFF" layer before joining the principal arbor. This morphology is characteristic of the ON direction selective (ON-DS) RGC, which has been extensively characterized both physiologically and morphologically in the mouse (Sun et al., 2006; Yonehara et al., 2008; Yonehara et al., 2009). *Brn3a*$^{AP/+}$ RGCs also include flat "ON" RGCs with small areas (e.g. cell k) that are not seen among *Brn3b*$^{AP/+}$ or *Brn3c*$^{AP/+}$ RGCs.

3.5 RGCs with bistratified arbors

Bistratified RGCs with stratification levels characteristic of ON-OFF direction selective cells are commonly observed among *Brn3a*$^{AP/+}$ and *Brn3c*$^{AP/+}$ RGCs but rarely observed among *Brn3b*$^{AP/+}$ RGCs (e.g., cells h, l, and m; see also Figs. 1G and 4). The few *Brn3b*$^{AP/+}$ bistratified RGCs analyzed here have, on average, larger inner dendritic arbor areas than *Brn3a*$^{AP/+}$ and *Brn3c*$^{AP/+}$ RGCs (Fig. 4B). In comparing reconstructed cells l and m, a distinction between bistratified *Brn3a*$^{AP/+}$ and *Brn3c*$^{AP/+}$ RGCs becomes apparent. Whereas in cell l, all "ON" dendrites are derived from the cell body or other "ON" dendrites (drawn

in blue), in cell m, about 50 % of "ON" stratifying dendrites derive from dendrites that had already descended into the "OFF" arbor and then looped back into the "ON" strata (drawn in gray). Although not quantified, this seems to be a consistent finding, and it might have implications for the "ON" vs. "OFF" input computations happening in ON-OFF DS RGCs.

3.6 Changes in arbor area with retinal eccentricity

Whereas average dendritic arbor areas of "ON" and "OFF" *Brn3c*$^{AP/+}$ RGC populations are comparable (mean area of "ON" RGCs = 16,256 μm^2, SD = 8,159 μm^2; mean area of "OFF" RGCs = 18,067 μm^2, SD = 7,351 μm^2), both cell types display a roughly linear correlation between area and retinal eccentricity, as defined by the distance from the cell body to the optic disc (Fig. 3D; for "ON" RGCs, R = 0.694, P = 1.755 e^{-7}; for "OFF" RGCs, R = 0.784, P = 1.6 e^{-5}). The analogous *Brn3a*$^{AP/+}$ and *Brn3b*$^{AP/+}$ scatter plots in Fig. 3D suggest a similar trend, although the greater heterogeneity of these RGC populations would be expected to partially obscure any strong eccentricity trend that is limited to one or a few RGC subtypes. This is, to our knowledge, the first report of an eccentricity effect in dendritic arbor areas for mouse RGCs. Interestingly, the variation in area is quite large, comprising an average change of ~2-fold between 0.5 and 1.5 mm eccentricity.

3.7 Effect of deleting individual Brn3 genes on RGC morphology

What are the consequences of deleting Brn3 transcription factors on the morphologies of individual RGCs? Previously, we reported major axon arbor defects in *Pax6αCre;Brn3b*$^{AP/-}$ RGCs and the loss of specific dendritic arbor morphologies together with an increase in the proportion of bistratified RGCs in *Pax6αCre;Brn3a*$^{AP/-}$ retinas (Badea et al., 2009a). These phenotypes are independently confirmed in the current study (Figs. 1D–G, 2D, 3, and 4; Table 2). We also observe here a higher proportion of bistratified dendritic morphologies among *Brn3b*$^{AP/-}$ RGCs compared to *Brn3b*$^{AP/+}$ RGCs (Fig. 1G; Table 2). The small decrease in the proportion of bistratified dendritic morphologies among *Brn3c*$^{AP/-}$ RGCs compared to *Brn3c*$^{AP/+}$ RGCs (Fig. 2G) is not statistically significant and, indeed, no statistically significant differences in RGC morphologies were observed between *Brn3c*$^{AP/+}$ and *Brn3c*$^{AP/-}$ samples with any of the parameters we measured (Figs. 3 and 4).

When *Brn3a* is removed from individual RGCs by sparse, *R26*^{rtTACreER}-induced recombination, surviving *Brn3a*$^{AP/-}$ cells encompass four basic morphologies: bistratified RGCs (e.g., cells p–r), flat "ON" or "OFF" RGCs (mostly costratifying with the 0.4 and 0.7 starburst amacrine cell landmarks), and sector cells. These data are in good agreement with our previous analysis of RGC morphologies in *Pax6αCre*; *Brn3a*$^{AP/-}$ retinas, and they support our previous suggestion that Brn3a may be necessary for the establishment of RGCs with small and thick dendritic arbors (cells d, e, and j; Badea et al 2009a). Interestingly, among bistratified *Brn3a*$^{AP/-}$ RGCs, many exhibit relatively simplified "ON" dendritic arbors, that expand into isolated and separated "OFF" arbors (compare cells p–r with cells e and l).

Many of the sparsely recombined *Brn3b*$^{AP/-}$ RGCs observed in this study exhibit the same abnormal features observed in *Pax6αCre;Brn3b*$^{AP/-}$ retinas, such as bifurcated axons penetrating in the IPL (Figs. 1E and F, and cell v), and small dendritic arbors arising from axonless cell bodies in the INL. The finding of amacrine or amacrine-like *Brn3b*$^{AP/-}$ (but not *Brn3b*$^{AP/+}$) neurons is consistent with a role for Brn3b in suppressing amacrine cell fates (Qiu et al., 2008). Stratification levels and areas of monostratified *Brn3b*$^{AP/-}$ dendritic arbors overlap substantially with those of *Brn3b*$^{AP/+}$ (Fig. 3) except for the presence of a subset of *Brn3b*$^{AP/-}$ RGCs with wide and thick arbors (e.g. cells t–v). These cells resemble the large "ON" morphologies seen both among *Brn3b*$^{AP/+}$ and *Brn3b*$^{AP/-}$ RGCs, except that individual *Brn3b*$^{AP/-}$ arbors encompass multiple IPL strata (compare cells g and u). In some

cases, these arbors resemble those of large bistratified Melanopsin cells (e.g., cell s; Berson et al., 2010).

As noted above, a striking, and previously unreported, observation is the expansion in the fraction of bistratified RGCs among *Brn3b*$^{AP/-}$ RGCs compared to *Brn3b*$^{AP/+}$ RGCs (Figs. 1G and 4). The majority of these bistratified neurons have inner arbors stratifying proximal to the 0.4 IPL landmark and outer arbors stratifying distal the 0.7 IPL landmark. Thus, the two dendritic arbor strata are further apart than is typical for ON-OFF DS bistratified RGCs (compare cells l and m with cell s) and do not coincide with the ChAT IPL bands. Moreover, in a subset of these RGCs, the cell bodies are offset from the dendritic arbor in a manner reminiscent of the monostratified sector cells (cells c, w, and x). To quantify this phenomenon, we computed the relative offset of the cell body in relation to the dendritic arbors for all inner and outer arbors of bistratified RGCs (Fig. 4C). The asymmetry parameter – defined as the distance between the cell body and the center of mass of the bounding polygon of either the inner or outer dendritic arbor, divided by the mean radius of the bounding polygon - is 0 for a perfectly symmetrical cell with a centered cell body, 1 for a cell body placed on the circumference of a circular bounding polygon, and greater than one for a cell body positioned beyond the circumference of a circular bounding polygon. Fig. 4C shows the extended distribution of asymmetry parameters calculated for *Brn3b*$^{AP/-}$ dendritic arbors, with a large fraction having values larger than 1.

4. Discussion

4.1 Patterns of Brn3 transcription factor expression and the division of RGCs into subtypes

How many types of RGCs are there in the mouse retina? Depending on the imaging approach, the parameters measured, and the clustering algorithms applied, estimates for morphologic types vary widely: 17 in Sun et al. 2002, 11 in Badea and Nathans, 2004, 11 in Kong et al., 2005, 14 in Coombs et al., 2006, and 22 in Volgyi et al., 2009. In the present study, at least 15 distinct RGC morphologies are visualized by using sparse recombination in the three *Brn3*$^{CKOAP/+}$ mouse lines.

These estimates represent a lower bound for a full classification system, as each morphological class could encompass multiple functional classes. Well-documented examples of this situation are bistratified ON-OFF DS cells, which have similar morphological parameters, yet can be differentiated by their preference for four distinct directions of stimulus movement (Barlow et al., 1964; Weng et al., 2005). For ON-OFF DS cells, dendritic arbor reconstructions using genetically driven reporters have recently been described (Schubert et al., 2005b; Huberman et al., 2009). Interestingly, Huberman et al report transgenic labeling of ON-OFF DS cells selectively responsive to stimuli moving in one direction, raising the possibility that the four functional ON-OFF DS RGCs subtypes might express distinctive molecular markers. More subtle distinctions between bistratified RGCs based on the number of recurrent dendrites looping from the “OFF” arbor to the “ON” arbor, as seen in comparing *Brn3a*$^{AP/+}$ RGC l and *Brn3c*$^{AP/+}$ RGC m, may add additional categories of ON-OFF bistratified RGCs.

Monostratified ON-DS RGCs (e.g., cell a), although morphologically indistinguishable from each other, also comprise three distinct functional classes, responsive to moving stimuli in three directions, “up”, “forward” and “backward”. These cells provide the afferent signals for the visual component of the vestibulo-ocular reflex, are labeled in *Brn3a*$^{CKOAP/+}$ and *Brn3b*$^{CKOAP/+}$ but not *Brn3c*$^{CKOAP/+}$ retinas, and project to three brainstem nuclei in the accessory optic system (Simpson, 1984; Yonehara et al., 2008; Badea et al., 2009a; Yonehara et al., 2009). The recent reports by Yonehara et al suggest that, within this

morphological group, there is molecular diversity that correlates with functional diversity. By contrast, the sector cells present among *Brn3a*$^{AP/+}$ and *Brn3b*$^{AP/+}$ RGCs (e.g., cell c), appear to constitute a unique type, identifiable by physiology, morphology and JamB expression (Kim et al., 2008).

In our data set, cells with morphologies similar to melanopsin-expressing RGCs are seen exclusively in *Brn3b*$^{CKOAP/+}$ retinas (cells f, g, and i; Hattar et al., 2002; Berson et al., 2010). This is consistent with the previous observation that *Brn3b*$^{AP/+}$ RGCs project to the OPN and IGL, and show a weak projection to the SCN, all of which are targets of melanopsin RGCs, whereas *Brn3a*$^{AP/+}$ and *Brn3c*$^{AP/+}$ RGCs avoid many of these targets (Badea et al., 2009a; Badea, Williams, Smallwood, and Nathans, manuscript in preparation).

The physiologic and morphologic properties, as well as one genetic marker, have been described for mouse “OFF” alpha RGCs (Pang et al., 2003; Schubert et al., 2005a; Völgyi et al., 2005; Huberman et al., 2008). This type is likely present in both *Brn3a*$^{AP/+}$ and *Brn3b*$^{AP/+}$ RGC data sets, exemplified by cell b, based on dendritic area and stratification, and the relatively straight, acutely angled dendrites. The flat monostratified “OFF” RGC type (cell o), is the only morphological type shared by all *Brn3*$^{AP/+}$ RGCs and represents the only “OFF” RGC labeled among *Brn3c*$^{AP/+}$ RGCs.

Cells with small and thick dendritic arbors (cells d and j) have been previously reported (Sun et al., 2002; Badea and Nathans, 2004; Coombs et al., 2006; Volgyi et al., 2009). We speculate that they represent the mouse beta RGCs, since they come in both “ON” (cell d) and “OFF” (cell j) variants, and stratify close to the middle of the IPL. These cells likely correspond to the small thick arbor clusters G5, G8, G13 and G14 described by Volgyi 2009. We note that similar RGCs with small areas and similar stratification levels have been reported as bistratified in Schubert et al., 2005b. In the present study, it is difficult to discern two arbors.

Another morphology present among both *Brn3a*$^{AP/+}$ and *Brn3b*$^{AP/+}$ RGCs, which is difficult to match with previously described morphologies, is exemplified by cell e. It most likely is classified as a bistratified RGC in Coombs et al., 2006, and is a member of cluster 5 in Badea and Nathans, 2004. In all of the examples of this RGC type in our data set and in the literature, the “OFF” arbor is sparser than the “ON” arbor, and “OFF” dendrites ascend vertically from the “ON” plexus to the inner edge of the INL. Although the physiological properties of this cell have not been reported in the mouse retina, bistratified RGCs with a similarly large distance between the two arbors have been described as blue – yellow color opponent cells in the primate (Dacey and Lee, 1994; Crook et al., 2009), and as “uniformity detectors” in rabbit (Famiglietti, 2009). Bistratified cells similar to cell e have been shown not to be color opponent in guinea pigs, which, like mice, have some cones that co-express the short- and medium-wavelength pigments (Applebury et al., 2000; Yin et al., 2009).

Brn3c$^{AP/+}$ RGCs can be divided in three distinct morphologies with tightly clustered morphological parameters: an “ON” RGC (cell n), an “OFF” RGC (cell o), and a bistratified, most likely an “ON-OFF”, RGC (cell m). The dendritic arbor areas of all three cells exhibit a linear increase with eccentricity, implying a central-to-peripheral decrease in visual acuity for these three channels.

Brn3a$^{AP/+}$ and *Brn3b*$^{AP/+}$ RGCs each encompass at least 10 distinct cell morphologies, consistent with immunohistochemical data showing that each transcription factor is expressed in ~75% of all RGCs (Badea et al. 2009a). In the present study, five distinct cell morphologies (cells a–e) were observed to be shared among *Brn3a*$^{AP/+}$ and *Brn3b*$^{AP/+}$ RGCs, one (cell n) is shared between *Brn3a*$^{AP/+}$ and *Brn3c*$^{AP/+}$ RGCs, and one (cell o) is shared by all three *Brn3*$^{AP/+}$ RGCs. This pattern is consistent with the hypothesis that the

Brn3 transcription factors constitute a combinatorial code for RGC cell type specification. This pattern also holds for other molecular markers identified thus far. For example, the photopigment Melanopsin is expressed in several distinct RGC cell types (Berson et al., 2010; Ecker et al., 2010); the secreted Ig domain molecule Spig1 is expressed in one type of ON-DS RGC in most of the retina, but in virtually all RGCs in the dorsal arc as well as in some amacrine cells (Yonehara et al., 2008); the Ig domain adhesion molecule JamB is transiently expressed in sector-shaped, upward direction selective RGCs, but also in a population of amacrine cells (Kim et al., 2008); and a calretinin-GFP bacterial artificial chromosome (BAC) transgene is expressed in transient OFF alpha RGCs as well as in a subset of amacrine cells (Huberman et al., 2008). Thus, genetic labeling and/or manipulation of only a single neuronal cell type will likely require intersectional strategies for gene regulation, as have been used in mice (Badea et al., 2009b) and *Drosophila* (Potter et al., 2010).

Do labeled RGCs in $Brn3^{CKOAP/+}$ retinas cover the entire spectrum of RGC types in the mouse? For at least one cell population, the answer is no. As previously reported, the SCN is not targeted by axons from $Brn3a^{AP/+}$ and $Brn3c^{AP/+}$ RGCs and only weakly innervated in its latero-caudal aspect by $Brn3b^{AP/+}$ RGCs (Badea et al., 2009a; Badea, Williams, Smallwood, and Nathans, manuscript in preparation). Thus, at least one melanopsin-expressing, SCN-projecting cell population is Brn3 negative. Another RGC morphology that appears to be absent from the Brn3 collection is the parvalbumin-5 “approach detecting” RGC described by Münch et al. (2009).

4.2 The role of Brn3 transcription factors in RGC specification

What are the roles of Brn3 transcription factors in RGC development? Previous reports indicated that Brn3b plays a role in RGC axon development, whereas Brn3a is involved in differentiation of dendritic arbors (Erkman et al., 1996; Gan et al., 1996; Erkman et al., 2000; Wang et al., 2000; Badea et al., 2009a). The current study confirms and extends these findings. First, we observe axon branching defects in individual, sparsely labeled $Brn3b^{AP/-}$ RGCs, as well as small, axonless amacrine-like $Brn3b^{AP/-}$ cells in the INL. Since more than 99 % of RGCs in these retinas are phenotypically WT (i.e. they have not undergone Cre-mediated recombination), these findings indicate that the aberrant morphologies are not caused by a defect at the optic nerve, in cues for axon path-finding, or in any other non-cell autonomous processes, but rather are the result of cell-autonomous defects secondary to Brn3b ablation. Second, among $Brn3b^{AP/-}$ RGCs with novel morphologies, there is a population with large arbor areas and dendrites that populate multiple IPL laminae (e.g., cells t and v). In general, RGC dendritic arbor area is anticorrelated with arbor thickness, so that RGCs that integrate signals over a large retinal area usually occupy a narrow stratum of the IPL, thereby receiving input from relatively limited bipolar and amacrine cell populations. By contrast, a significant fraction of RGCs with small dendritic arbor areas collect information from several IPL strata, and could therefore receive synaptic inputs from a broader population of bipolar and amacrine cell types. Finally, a class of $Brn3b^{AP/-}$ RGCs with abnormal dendritic arbor morphologies is seen in the expanded population of AP-expressing bistratified RGCs. Roughly half of these bistratified $Brn3b^{AP/-}$ RGCs exhibit extremely asymmetric dendritic arbors, reminiscent of the sector/JamB population of monostratified RGCs (cells w, x). These asymmetries could plausibly arise from abnormal cell body movements among otherwise normal bistratified RGCs, or they could derive from sector RGCs that have developed a second dendritic arbor.

Acknowledgments

Supported by the Howard Hughes Medical Institute.

References

Amthor FR, Oyster CW, Takahashi ES. Morphology of on-off direction-selective ganglion cells in the rabbit retina. Brain Res. 1984; 298(1):187–190. [PubMed: 6722555]

Applebury ML, Antoch MP, Baxter LC, Chun LL, Falk JD, Farhangfar F, Kage K, Krzystolik MG, Lyass LA, Robbins JT. The murine cone photoreceptor: a single cone type expresses both S and M opsins with retinal spatial patterning. Neuron. 2000; 27:513–523. [PubMed: 11055434]

Badea TC, Wang Y, Nathans J. A noninvasive genetic/pharmacologic strategy for visualizing cell morphology and clonal relationships in the mouse. J Neurosci. 2003; 23:2314–2322. [PubMed: 12657690]

Badea TC, Nathans J. Quantitative analysis of neuronal morphologies in the mouse retina visualized by using a genetically directed reporter. J Comp Neurol. 2004; 480:331–351. [PubMed: 15558785]

Badea TC, Cahill H, Ecker J, Hattar S, Nathans J. Distinct roles of transcription factors brn3a and brn3b in controlling the development, morphology, and function of retinal ganglion cells. Neuron. 2009a; 61:852–864. [PubMed: 19323995]

Badea TC, Hua ZL, Smallwood PM, Williams J, Rotolo T, Ye X, Nathans J. New mouse lines for the analysis of neuronal morphology using CreER(T)/loxP-directed sparse labeling. PLoS One. 2009b; 4:e7859. [PubMed: 19924248]

Barlow HB, Hill RM, Levick WR. Retinal ganglion cells responding selectively to direction and speed of image motion in the rabbit. J Physiol. 1964; 173:377–407. [PubMed: 14220259]

Berson DM, Dunn FA, Takao M. Phototransduction by retinal ganglion cells that set the circadian clock. Science. 2002; 295:1070–1073. [PubMed: 11834835]

Berson DM, Castrucci AM, Provencio I. Morphology and mosaics of melanopsin-expressing retinal ganglion cell types in mice. J Comp Neurol. 2010; 518:2405–2422. [PubMed: 20503419]

Boycott BB, Wassle H. The morphological types of ganglion cells of the domestic cat's retina. J Physiol. 1974; 240:397–419. [PubMed: 4422168]

Carcieri SM, Jacobs AL, Nirenberg S. Classification of retinal ganglion cells: a statistical approach. J Neurophysiol. 2003; 90:1704–1713. [PubMed: 12966177]

Cleland BG, Levick WR. Brisk and sluggish concentrically organized ganglion cells in the cat's retina. J Physiol. 1974a; 240:421–456. [PubMed: 4421622]

Cleland BG, Levick WR. Properties of rarely encountered types of ganglion cells in the cat's retina and an overall classification. J Physiol. 1974b; 240:457–492. [PubMed: 4420300]

Coombs J, van der List D, Wang G, Chalupa LM. Morphological properties of mouse retinal ganglion cells. Neuroscience. 2006; 140:123–136. [PubMed: 16626866]

Crook JD, Davenport CM, Peterson BB, Packer OS, Detwiler PB, Dacey DM. Parallel ON and OFF cone bipolar inputs establish spatially coextensive receptive field structure of blue-yellow ganglion cells in primate retina. J Neurosci. 2009; 29:8372–8387. [PubMed: 19571128]

Dacey DM, Lee BB. The 'blue-on' opponent pathway in primate retina originates from a distinct bistratified ganglion cell type. Nature. 1994; 367:731–735. [PubMed: 8107868]

Dacey DM, Peterson BB, Robinson FR, Gamlin PD. Fireworks in the primate retina: in vitro photodynamics reveals diverse LGN-projecting ganglion cell types. Neuron. 2003; 37:15–27. [PubMed: 12526769]

Do MT, Kang SH, Xue T, Zhong H, Liao H, Bergles DE, Yau K. Photon capture and signalling by melanopsin retinal ganglion cells. Nature. 2009; 457:281–287. [PubMed: 19118382]

Ecker JL, Dumitrescu ON, Wong KY, Alam NM, Chen SK, LeGates T, Renna JM, Prusky JT, Berson DM, Hattar S. Melanopsin-expressing retinal ganglioncell photoreceptors: cellular diversity and role in pattern vision. Neuron. 2010 Jul; 67(1):49–60. [PubMed: 20624591]

Erkman L, McEvilly RJ, Luo L, Ryan AK, Hooshmand F, O'Connell SM, Keithley EM, Rapaport DH, Ryan AF, Rosenfeld MG. Role of transcription factors Brn-3.1 and Brn-3.2 in auditory and visual system development. Nature. 1996; 381:603–606. [PubMed: 8637595]

Erkman L, Yates PA, McLaughlin T, McEvilly RJ, Whisenhunt T, O'Connell SM, Krones AI, Kirby MA, Rapaport DH, Bermingham JR, O'Leary DD, Rosenfeld MG. A POU domain transcription factor-dependent program regulates axon pathfinding in the vertebrate visual system. Neuron. 2000; 28:779–792. [PubMed: 11163266]

Euler T, Schneider H, Wassle H. Glutamate responses of bipolar cells in a slice preparation of the rat retina. J Neurosci. 1996; 16:2934–2944. [PubMed: 8622124]

Famiglietti EV, Kolb H. Structural basis for ON-and OFF-center responses in retinal ganglion cells. Science. 1976; 194:193–195. [PubMed: 959847]

Famiglietti EV. Bistratified ganglion cells of rabbit retina: Neural architecture for contrast-independent visual responses. Vis Neurosci. 2009:1–19. [PubMed: 19347975]

Fuerst PG, Koizumi A, Masland RH, Burgess RW. Neurite arborization and mosaic spacing in the mouse retina require DSCAM. Nature. 2008; 451:470–474. [PubMed: 18216855]

Fuerst PG, Bruce F, Tian M, Wei W, Elstrott J, Feller MB, Erskine L, Singer JH, Burgess RW. DSCAM and DSCAML1 function in self-avoidance in multiple cell types in the developing mouse retina. Neuron. 2009; 64:484–497. [PubMed: 19945391]

Gan L, Xiang M, Zhou L, Wagner DS, Klein WH, Nathans J. POU domain factor Brn-3b is required for the development of a large set of retinal ganglion cells. Proc Natl Acad Sci U S A. 1996; 93:3920–3925. [PubMed: 8632990]

Ghosh KK, Bujan S, Haverkamp S, Feigenspan A, Wassle H. Types of bipolar cells in the mouse retina. J Comp Neurol. 2004; 469:70–82. [PubMed: 14689473]

Guler AD, Ecker JL, Lall GS, Haq S, Altimus CM, Liao H, Barnard AR, Cahill H, Badea TC, Zhao H, Hankins MW, Berson DM, Lucas RJ, Yau K, Hattar S. Melanopsin cells are the principal conduits for rod-cone input to non-image-forming vision. Nature. 2008; 453:102–105. [PubMed: 18432195]

Hattar S, Liao HW, Takao M, Berson DM, Yau KW. Melanopsin-containing retinal ganglion cells: architecture, projections, and intrinsic photosensitivity. Science. 2002; 295:1065–1070. [PubMed: 11834834]

Haverkamp S, Wassle H. Immunocytochemical analysis of the mouse retina. J Comp Neurol. 2000; 424:1–23. [PubMed: 10888735]

Huberman AD, Manu M, Koch SM, Susman MW, Lutz AB, Ullian EM, Baccus SA, Barres BA. Architecture and activity-mediated refinement of axonal projections from a mosaic of genetically identified retinal ganglion cells. Neuron. 2008; 59:425–438. [PubMed: 18701068]

Huberman AD, Wei W, Elstrott J, Stafford BK, Feller MB, Barres BA. Genetic identification of an On-Off direction-selective retinal ganglion cell subtype reveals a layer-specific subcortical map of posterior motion. Neuron. 2009; 62:327–334. [PubMed: 19447089]

Kim I, Zhang Y, Yamagata M, Meister M, Sanes JR. Molecular identification of a retinal cell type that responds to upward motion. Nature. 2008; 452:478–482. [PubMed: 18368118]

Kim I, Zhang Y, Meister M, Sanes JR. Laminar restriction of retinal ganglion cell dendrites and axons: subtype-specific developmental patterns revealed with transgenic markers. J Neurosci. 2010; 30:1452–1462. [PubMed: 20107072]

Kong J, Fish DR, Rockhill RL, Masland RH. Diversity of ganglion cells in the mouse retina: unsupervised morphological classification and its limits. J Comp Neurol. 2005; 489:293–310. [PubMed: 16025455]

Levick WR. Receptive fields and trigger features of ganglion cells in the visual streak of the rabbits retina. J Physiol. 1967; 188:285–307. [PubMed: 6032202]

Levick WR. Form and function of cat retinal ganglion cells. Nature. 1975; 254:659–662. [PubMed: 47614]

Masland RH. Neuronal diversity in the retina. Curr Opin Neurobiol. 2001; 11:431–436. [PubMed: 11502388]

Masland RH, Martin PR. The unsolved mystery of vision. Curr Biol. 2007; 17:R577–R582. [PubMed: 17686423]

Morgan JL, Dhingra A, Vardi N, Wong RO. Axons and dendrites originate from neuroepithelial-like processes of retinal bipolar cells. Nat Neurosci. 2006; 9:85–92. [PubMed: 16341211]

Münch TA, da Silveira RA, Siegert S, Viney TJ, Awatramani GB, Roska B. Approach sensitivity in the retina processed by a multifunctional neural circuit. Nat Neurosci. 2009; 12:1308–1316. [PubMed: 19734895]

Pang J, Gao F, Wu SM. Light-evoked excitatory and inhibitory synaptic inputs to ON and OFF alpha ganglion cells in the mouse retina. J Neurosci. 2003; 23:6063–6073. [PubMed: 12853425]

Potter CJ, Tasic B, Russler EV, Liang L, Luo L. The Q system: a repressible binary system for transgene expression, lineage tracing, and mosaic analysis. Cell. 2010; 141:536–548. [PubMed: 20434990]

Pu ML, Amthor FR. Dendritic morphologies of retinal ganglion cells projecting to the lateral geniculate nucleus in the rabbit. J Comp Neurol. 1990a; 302:675–693. [PubMed: 1702124]

Pu ML, Amthor FR. Dendritic morphologies of retinal ganglion cells projecting to the nucleus of the optic tract in the rabbit. J Comp Neurol. 1990b; 302:657–674. [PubMed: 1702123]

Qiu F, Jiang H, Xiang M. A comprehensive negative regulatory program controlled by Brn3b to ensure ganglion cell specification from multipotential retinal precursors. J Neurosci. 2008; 28:3392–3403. [PubMed: 18367606]

Ramon, y; Cajal, S. The structure of the retina. Springfield, Ill.: C.C. Thomas; 1972.

Rockhill RL, Daly FJ, MacNeil MA, Brown SP, Masland RH. The diversity of ganglion cells in a mammalian retina. J Neurosci. 2002; 22:3831–3843. [PubMed: 11978858]

Rodieck RW, Watanabe M. Survey of the morphology of macaque retinal ganglion cells that project to the pretectum, superior colliculus, and parvicellular laminae of the lateral geniculate nucleus. J Comp Neurol. 1993; 338:289–303. [PubMed: 8308173]

Roska B, Werblin F. Vertical interactions across ten parallel, stacked representations in the mammalian retina. Nature. 2001; 410:583–587. [PubMed: 11279496]

Schubert T, Degen J, Willecke K, Hormuzdi SG, Monyer H, Weiler R. Connexin36 mediates gap junctional coupling of alpha-ganglion cells in mouse retina. J Comp Neurol. 2005a; 485:191–201. [PubMed: 15791644]

Schubert T, Maxeiner S, Kruger O, Willecke K, Weiler R. Connexin45 mediates gap junctional coupling of bistratified ganglion cells in the mouse retina. J Comp Neurol. 2005b; 490:29–39. [PubMed: 16041717]

Siegert S, Scherf BG, Del Punta K, Didkovsky N, Heintz N, Roska B. Genetic address book for retinal cell types. Nat Neurosci. 2009; 12:1197–1204. [PubMed: 19648912]

Simpson JI. The accessory optic system. Annu Rev Neurosci. 1984; 7:13–41. [PubMed: 6370078]

Sun W, Li N, He S. Large-scale morphological survey of mouse retinal ganglion cells. J Comp Neurol. 2002; 451:115–126. [PubMed: 12209831]

Sun W, Deng Q, Levick WR, He S. ON direction-selective ganglion cells in the mouse retina. J Physiol. 2006; 576:197–202. [PubMed: 16901944]

Troy JB, Shou T. The receptive fields of cat retinal ganglion cells in physiological and pathological states: where we are after half a century of research. Prog Retin Eye Res. 2002; 21:263–302. [PubMed: 12052385]

Volgyi B, Chheda S, Bloomfield SA. Tracer coupling patterns of the ganglion cell subtypes in the mouse retina. J Comp Neurol. 2009; 512:664–687. [PubMed: 19051243]

Wang SW, Gan L, Martin SE, Klein WH. Abnormal polarization and axon outgrowth in retinal ganglion cells lacking the POU-domain transcription factor Brn-3b. Mol Cell Neurosci. 2000; 16:141–156. [PubMed: 10924257]

Wang SW, Mu X, Bowers WJ, Kim D, Plas DJ, Crair MC, Federoff HJ, Gan L, Klein WH. Brn3b/Brn3c double knockout mice reveal an unsuspected role for Brn3c in retinal ganglion cell axon outgrowth. Development. 2002; 129:467–477. [PubMed: 11807038]

Wassle H. Parallel processing in the mammalian retina. Nat Rev Neurosci. 2004; 5:747–757. [PubMed: 15378035]

Weng S, Sun W, He S. Identification of ON-OFF direction-selective ganglion cells in the mouse retina. J Physiol. 2005; 562:915–923. [PubMed: 15564281]

Xiang M, Zhou L, Macke JP, Yoshioka T, Hendry SH, Eddy RL, Shows TB, Nathans J. The Brn-3 family of POU-domain factors: primary structure, binding specificity, and expression in subsets of retinal ganglion cells and somatosensory neurons. J Neurosci. 1995; 15:4762–4785. [PubMed: 7623109]

Xiang M, Gan L, Li D, Chen ZY, Zhou L, O'Malley BW Jr, Klein W, Nathans J. Essential role of POU-domain factor Brn-3c in auditory and vestibular hair cell development. Proc Natl Acad Sci U S A. 1997; 94:9445–9450. [PubMed: 9256502]

Xiang M, Gan L, Zhou L, Klein WH, Nathans J. Targeted deletion of the mouse POU domain gene Brn-3a causes selective loss of neurons in the brainstem and trigeminal ganglion, uncoordinated limb movement, and impaired suckling. Proc Natl Acad Sci U S A. 1996; 93:11950–11955. [PubMed: 8876243]

Yamagata M, Weiner JA, Sanes JR. Sidekicks: synaptic adhesion molecules that promote lamina-specific connectivity in the retina. Cell. 2002; 110:649–660. [PubMed: 12230981]

Yamagata M, Sanes JR. Dscam and Sidekick proteins direct lamina-specific synaptic connections in vertebrate retina. Nature. 2008; 451:465–469. [PubMed: 18216854]

Yin L, Smith RG, Sterling P, Brainard DH. Physiology and morphology of color-opponent ganglion cells in a retina expressing a dual gradient of S and M opsins. J Neurosci. 2009; 29:2706–2724. [PubMed: 19261865]

Yonehara K, Shintani T, Suzuki R, Sakuta H, Takeuchi Y, Nakamura-Yonehara K, Noda M. Expression of SPIG1 reveals development of a retinal ganglion cell subtype projecting to the medial terminal nucleus in the mouse. PLoS ONE. 2008; 3:e1533. [PubMed: 18253481]

Yonehara K, Ishikane H, Sakuta H, Shintani T, Nakamura-Yonehara K, Kamiji NL, Usui S, Noda M. Identification of retinal ganglion cells and their projections involved in central transmission of information about upward and downward image motion. PLoS One. 2009; 4:e4320. [PubMed: 19177171]

Zeck GM, Masland RH. Spike train signatures of retinal ganglion cell types. Eur J Neurosci. 2007; 26:367–380. [PubMed: 17650112]

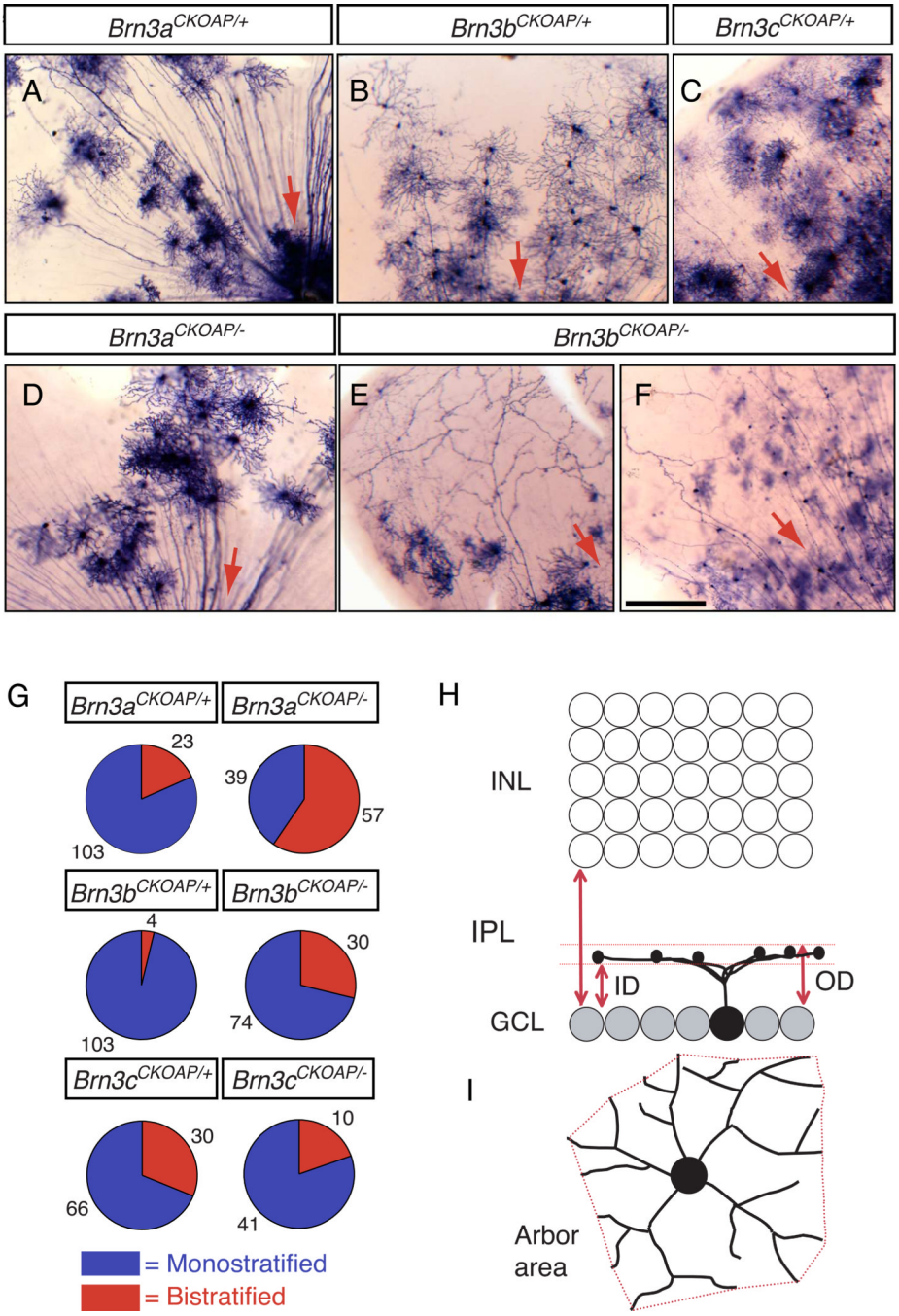

Fig. 1. Mouse RGCs visualized by sparse recombination of conditional AP reporter knock-in alleles at the *Brn3a, Brn3b,* and *Brn3c* loci

(A–F) Flat mount preparations of retinas from (A) $R26^{rtTACreER/+}$;$Brn3a^{CKOAP/+}$, (B) $R26^{rtTACreER/+}$;$Brn3b^{CKOAP/+}$, (C) $R26^{rtT\text{-}CreER/+}$;$Brn3c^{CKOAP/+}$, (D) $R26^{rtTACreER/+}$;$Brn3a^{CKOAP/-}$, and (E,F) $R26^{rtTACreER/+}$;$Brn3b^{CKOAP/-}$ mice, histochemically stained for AP activity. Red arrows indicate the direction of the optic disc. (G) Pie charts showing the ratios of monostratified (blue): bistratified (red) RGCs from retinas of the indicated genotypes. The number of cells of each type is indicated. (H,I), Morphological parameters for the analysis of RGC dendritic arbors. In (H), the inner distance (ID) and outer distance (OD), normalized to the IPL thickness, together define the

level of arbor stratification and thickness. ID and OD equal 0 at the level of the ganglion cell layer, and they equal 1 at the level of the INL. In (I), the arbor area is calculated as the area of the polygon (in red) with the shortest perimeter that connects the tips of the RGC dendrites when projected in the plane of the retina. Scale bar in F, 100 μm.

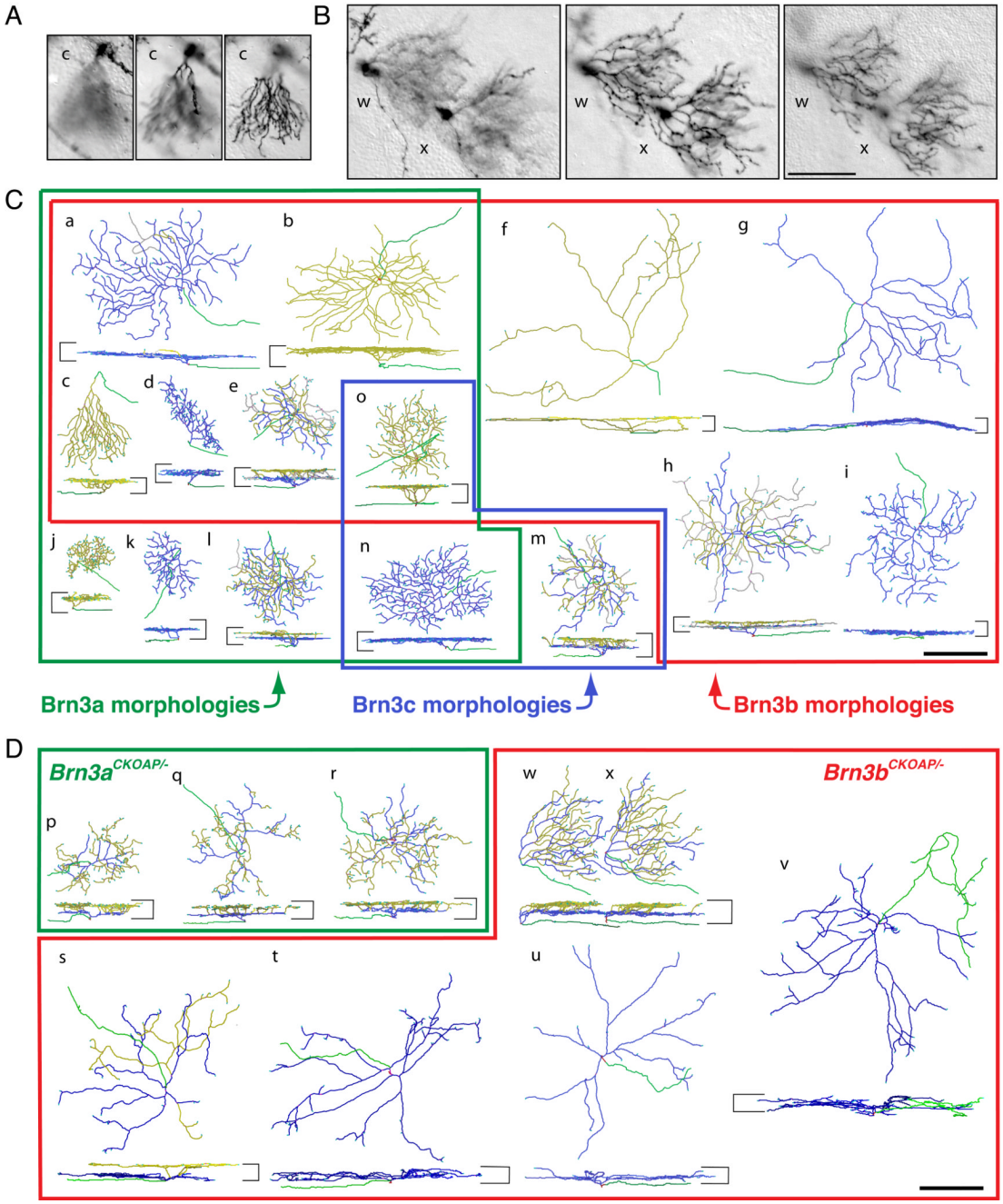

Fig. 2. Examples of the morphologies of WT and mutant RGCs expressing each of the three *Brn3*^{AP} alleles

(A,B) Sequential z-dimension DIC images of one *Brn3b*$^{AP/+}$ (A) and two *Brn3b*$^{AP/-}$ (B) RGCs in flat mounted retinas. The planes of the optical sections are at the nerve fiber layer (left panels), at ~0.3–0.4 IPL depth (central panels) and at the boundary of the IPL and INL (right panels). The images in (A) and (B) correspond, respectively, to reconstructed cell c in panel (C) and reconstructed cells w and x in panel (D). For cell c, the dendrites stratify adjacent to the INL, whereas for cells w and x there are two distinct arbors (coded blue and yellow in (D)), one stratifying at an IPL depth of ~0.35 and the second stratifying adjacent to the INL. (C,D) Reconstructions of individual *Brn3*$^{AP/+}$ (C) and *Brn3*$^{AP/-}$ (D) RGCs

obtained from DIC z-stacks similar to the ones sampled in panels (A–B). For each cell, *en face* (top) and vertical views (bottom) are shown. The boundaries of the IPL are shown as horizontal bars on the sides of each vertical projection. Axons are green, vitreal ("ON") dendrites are blue, and scleral ("OFF") dendrites are yellow. "Recurrent" dendrites, defined as originating in the scleral plexus and ending in the vitreal plexus, are gray (present in cells a, e, h, l, and m). (C) Distinct RGC morphological types representative of the $Brn3a^{AP/+}$, $Brn3b^{AP/+}$ and $Brn3c^{AP/+}$ data sets are enclosed in green, red and blue outlines, respectively. Types j, k, and l are unique to $Brn3a^{AP/+}$ RGCs; types f, g, h and i to $Brn3b^{AP/+}$ RGCs; and type m to $Brn3c^{AP/+}$ RGCs. Types a–e are observed among both $Brn3a^{AP/+}$ and $Brn3b^{AP/+}$ RGCs; type n in $Brn3a^{AP/+}$ and $Brn3c^{AP/+}$ RGCs; and type o in all three $Brn3^{AP/+}$ RGCs. The specific examples shown are derived from $Brn3a^{CKOAP/+}$ (a, b, e, j, k, l, n), $Brn3b^{CKOAP/+}$ (c, d, f, g, h, i, o) and $Brn3c^{CKOAP/+}$ (m) retinas. (D) Examples of RGC morphologies observed in the $Brn3a^{CKOAP/-}$ and $Brn3b^{CKOAP/-}$ retinas are enclosed in green and red outlines, respectively. Examples of bistratified $Brn3a^{AP/-}$ RGCs (p, q, r), bistratified $Brn3b^{AP/-}$ RGCs (s, w, x) and monostratified $Brn3b^{AP/-}$ RGCs (t, u, v) are shown. Scale bars in B, C and D, 100 μm.

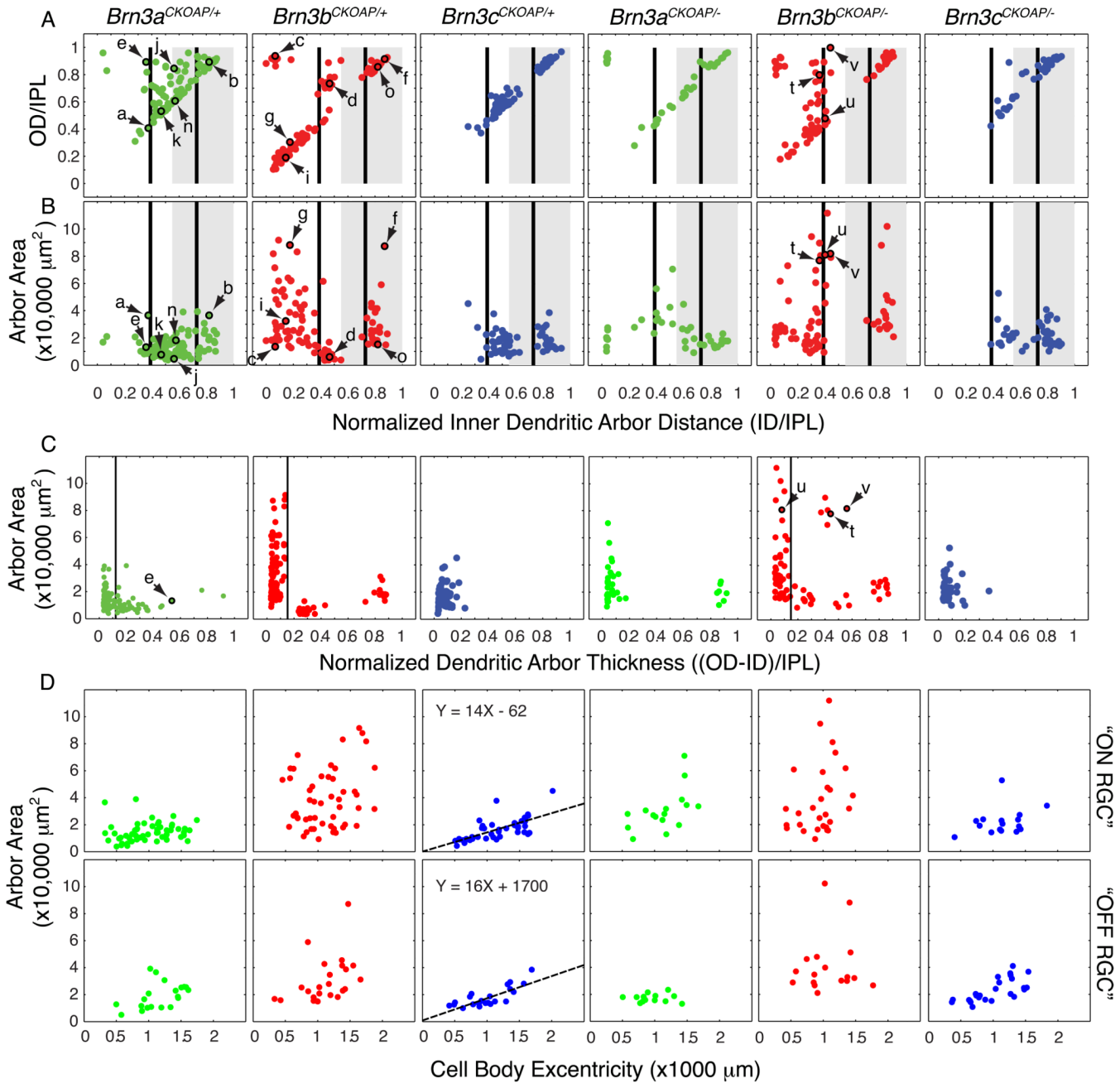

Fig. 3. Morphological parameters for monostratified *Brn3*$^{AP/+}$ and *Brn3*$^{AP/-}$ RGCs

Scatter plots in each vertical column refer to RGCs with the genotypes indicated at the top. Arrows and lower case letters identify the cells shown in Fig. 2. (A,B) Scatter plots of normalized inner distance (ID/IPL) vs. normalized outer distance (OD/IPL) and ID/IPL vs. dendritic arbor area. These parameters are defined in Fig. 1 H and I. The black vertical bars at 0.39 and 0.73 ID/IPL (referred to in the text as ~0.4 and ~0.7, respectively) represent the stratification levels of the "ON" (0.39) and "OFF" (0.73) bands of calretinin, calbindin, and choline acetyltransferase immunostaining, as measured by Haverkamp and Wassle (2000),Morgan et al. (2006), and Badea et al. (2009a). The grey rectangle spanning 0.55–1.0 ID/IPL represents the "OFF" sublamina of the IPL, as determined by the stratification level

of the central band of calretinin/calbindin immunoreactivity (Haverkamp and Wassle, 2000;Badea et al 2009a) and of the axon arbor terminals of mGluR6-expressing, "ON" bipolar cells (Morgan et al 2006). (C) Scatter plots for the dendritic arbor thickness, (OD-ID)/IPL vs. arbor area. The dendritic arbor thickness represents the difference of the outer distance (OD) and inner distance (ID), as defined in Fig. 1H, normalized to the thickness of the IPL. (D) Dendritic arbor areas increase with eccentricity for flat monostratified *Brn3c*$^{AP/+}$ and *Brn3c*$^{AP/-}$ RGCs in the mouse retina. Scatter plots of eccentricity (distance of the cell body from the optic nerve head) vs. area for flat monostratified RGCs. Flat monostratified RGCs include all monostratified Brn3c$^{AP/+}$ RGCs, as well as *Brn3a*$^{AP/+}$ and *Brn3b*$^{AP/+}$ RGCs with normalized dendritic arbor thicknesses <0.12 and <0.15, respectively; these cutoffs are based on the positions of troughs in the arbor thickness distributions in panel C. For *Brn3a*$^{AP/+}$ and *Brn3b*$^{AP/+}$ RGCs, "ON" or "OFF" types were defined as having an ID/IPL ratio under or above 0.55, respectively. For *Brn3c*$^{AP/+}$ RGCs, cells close to the 0.55 ON/OFF border were grouped with the RGCs that clustered nearby in parameter space in panels A and B. There is a linear correlation between eccentricity and dendritic arbor area for both "ON" and "OFF" *Brn3c*$^{AP/+}$ and *Brn3c*$^{AP/-}$ RGCs, and the best fitting straight line is shown.

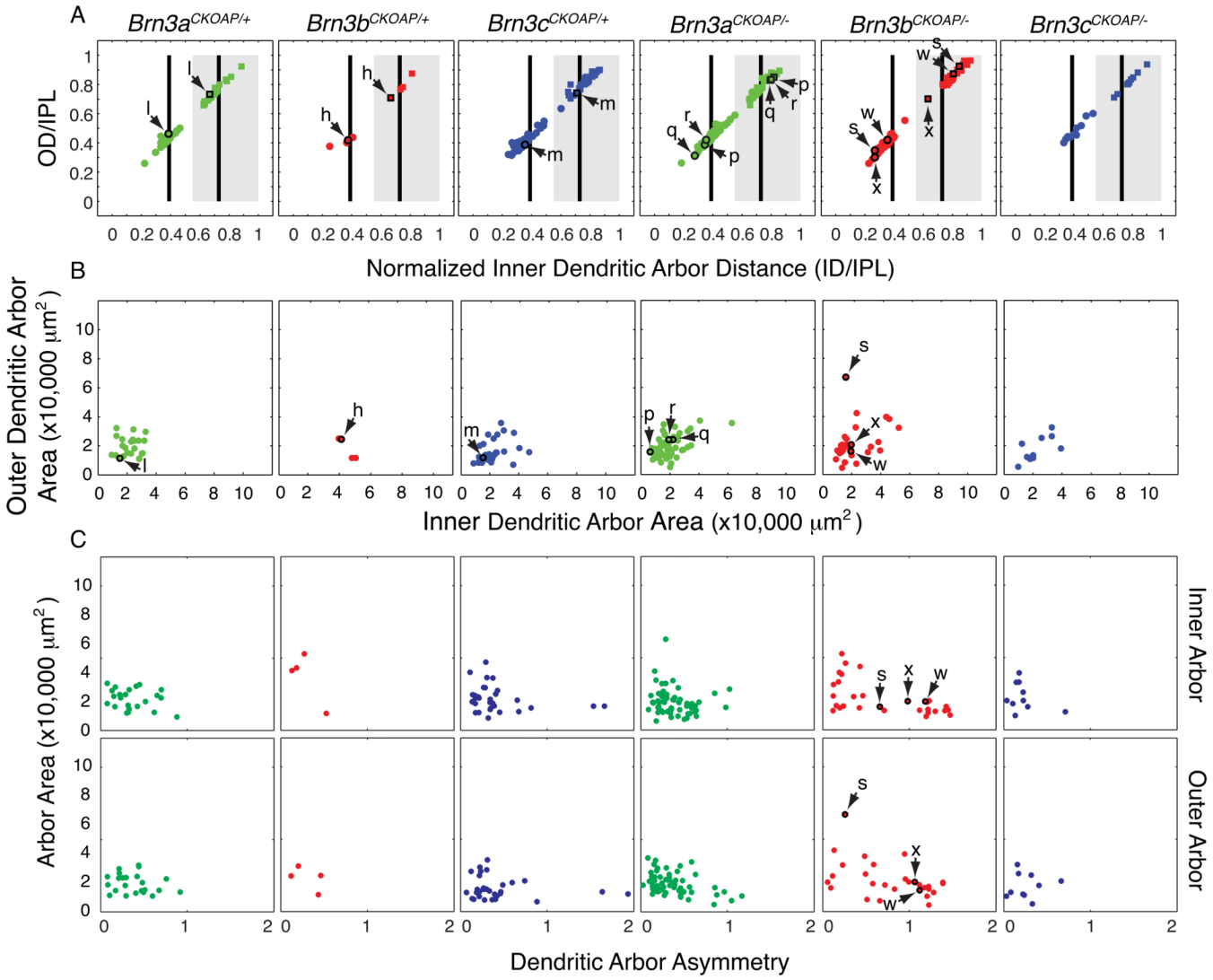

Fig. 4. Morphological parameters for bistratified *Brn3*$^{AP/+}$ and *Brn3*$^{AP/-}$ RGCs

Scatter plots in each vertical column refer to RGCs with the genotypes indicated at the top. Arrows and lower case letters identify the cells shown in Fig. 2. (A,B) Scatter plots of normalized inner distance (ID/IPL) vs. normalized outer distance (OD/IPL) and inner dendritic arbor area vs. outer dendritic arbor area. These parameters are defined in Fig. 1 H and I. For black vertical bars and gray rectangle landmarks in panel A, see Fig. 3 legend. In (A) stratification parameters for the inner dendritic arbors (circles) and outer dendritic arbors (squares) are plotted for each cell, e.g. inner and outer dendritic arbors for cell l, in the Brn3a$^{CKOAP/+}$ scatter plot are plotted as a circle and a square, highlighted by a black outline, and indicated by a pair of arrows. (C) Scatter plots of dendritic arbor asymmetry vs. arbor area, for inner (top) and outer (bottom) arbors. The asymmetry parameter is defined as the distance from the xy coordinates of the cell body to the center of mass of the bounding polygon of the dendritic arbor, normalized by the average radius of the bounding polygon.

Table 1

Doxycycline and 4-HT treatment

Brn3 locus genotype	Mouse tag[#]	Doxycycline regime	4 HT administration
Brn3a$^{CKOAP/+}$	8664	E4-P0 = 1	E11 = 150 microgr
	8640	E4-P0 = food	E13 = 100 microgr
	9015, 9018	E3-P2 = food	E12 = 200 microgr
	9030	E3-P5 = food	E12 = 250 microgr
Brn3a$^{CKOAP/-}$	8641, 8643	E4-P0 = food	E13 = 100 microgr
	9026, 9031	E3-P5 = food	E12 = 250 microgr
Brn3b$^{CKOAP/+}$	8740	E4-P0 = food	E12 = 200
	8753	E4-P0 = food	E11 = 100
Brn3b$^{CKOAP/-}$	8741	E4-P0 = food	E12 = 200
	8754	E4-P0 = food	E11 = 100
Brn3c$^{CKOAP/+}$	8881	E5-P0 = food	E14 = 400 microgr
	8933	E3-P0 = food	E13 = 250 microgr
	9058, 9171	E2-P0 = food	E12 = 200 microgr
Brn3c$^{CKOAP/-}$	8934, 8938	E3-P0 = food	E13 = 250 microgr

[#]For each mouse both retinas were analyzed.

Table 2

AP-expressing monostratified and bistratified RGCs

	monostratified	bistratified	total	monostratified %	Bistratified %
Brn3a$^{AP/+}$	103	23	126	82	18
Brn3a$^{AP/-}$	39	57	96	41	59
Brn3b$^{AP/+}$	103	4	107	96	4
Brn3b$^{AP/-}$	74	30	104	71	29
Brn3c$^{AP/+}$	66	30	96	69	31
Brn3c$^{AP/-}$	41	10	51	80	20